

Assessment of Uncertainties for the NIST 1016 mm Guarded-Hot-Plate Apparatus: Extended Analysis for Low-Density Fibrous-Glass Thermal Insulation

Author's Note: This paper is based on NIST Technical Note 1606, *Assessment of Uncertainties for the NIST 1016 mm Guarded-Hot-Plate Apparatus: Extended Analysis for Low-Density Fibrous-Glass Thermal Insulation*, February 2009. Most of the content remains the same; the uncertainty analysis has been updated to reflect recent modifications in the heat flow imbalance study (p. 44).

Volume 115

Number 1

January-February 2010

Robert R. Zarr

National Institute of Standards
and Technology,
Gaithersburg, MD 20899-8632

robert.zarr@nist.gov

An assessment of uncertainties for the National Institute of Standards and Technology (NIST) 1016 mm Guarded-Hot-Plate apparatus is presented. The uncertainties are reported in a format consistent with current NIST policy on the expression of measurement uncertainty. The report describes a procedure for determination of component uncertainties for thermal conductivity and thermal resistance for the apparatus under operation in either the double-sided or single-sided mode of operation. An extensive example for computation of uncertainties for the single-sided mode of operation is provided for a low-density fibrous-glass blanket thermal insulation. For this material, the relative expanded uncertainty for thermal resistance increases from 1 % for a thickness of 25.4 mm to 3 % for a thickness of 228.6 mm. Although these uncertainties have been developed for a particular insulation material, the procedure and, to a

lesser extent, the results are applicable to other insulation materials measured at a mean temperature close to 297 K (23.9 °C, 75 °F). The analysis identifies dominant components of uncertainty and, thus, potential areas for future improvement in the measurement process. For the NIST 1016 mm Guarded-Hot-Plate apparatus, considerable improvement, especially at higher values of thermal resistance, may be realized by developing better control strategies for guarding that include better measurement techniques for the guard gap thermopile voltage and the temperature sensors.

Key words: building technology; fibrous glass blanket; guarded hot plate; thermal conductivity; thermal insulation; thermal resistance; uncertainty.

Accepted: November 3, 2009

Available online: <http://www.nist.gov/jres>

1. Introduction

In October 1992, NIST officially adopted a new policy [1] for the expression of measurement uncertainty consistent with international practices. The NIST policy is based on recommendations by the Comité International des Poids et Mesures (CIPM) given in the *Guide to the Expression of Uncertainty in Measurement* [2] hereafter, called the GUM.¹ This report assesses the

¹ Certain commercial entities, equipment, or materials may be identified in this document in order to describe an experimental procedure or concept adequately. Such identification is not intended to imply recommendation or endorsement by the National Institute of Standards and Technology, nor is it intended to imply that the entities, materials, or equipment are necessarily the best available for the purpose.

uncertainties for the NIST 1016 mm Guarded-Hot-Plate apparatus and expresses the uncertainties in a manner consistent with NIST policy. The uncertainty assessment presented herein elaborates on a previous effort [3] presented in 1997 for the production of NIST Standard Reference Material (SRM) 1450c and supersedes the previous error analysis prepared by Rennex in 1983 [4]. Technical details of the apparatus design and fabrication have been described previously [5-6] and, therefore, are only briefly presented here.

The guarded-hot-plate method was standardized in 1945 after many years of effort and designated ASTM Test Method C 177 [7]. Essentially, the method establishes steady-state heat flow through flat homogeneous slabs—the surfaces of which are in contact with ad-

joining parallel boundaries (i.e., plates) maintained at constant temperatures. The method is considered an absolute measurement procedure because the resulting heat transmission coefficients are directly determined. That is, the test results are not determined by ratio of quantities. In principle, the method can be used over a range of temperatures but, in this report, the mean temperature is limited primarily to 297 K (23.9 °C, 75 °F). This report discusses the measurement principle and presents a procedure for the assessment of uncertainties for a particular lot of low-density fibrous-glass thermal insulation maintained by the NIST Building and Fire Research Laboratory (BFRL).

2. Reference Material

The reference material of interest in this report is a low-density fibrous-glass blanket having a nominal bulk density of $9.6 \text{ kg} \cdot \text{m}^{-3}$ ($0.6 \text{ lb} \cdot \text{ft}^{-3}$). The material lots were manufactured in July 1980 in the form of large sheets (1.2 m by 2.4 m) at nominal thicknesses of 28 mm and 81 mm. After receipt and preparation of the material, the National Bureau of Standards² announced in December 1980 a program [8] to provide thick “calibration transfer specimens” (CTS) on request for use in conjunction with the “representative thick-

ness” provision of the U.S. Federal Trade Commission (FTC) rules published in 1979 [9] hereafter, called the “R-value Rule.” The specimens were 610 mm square and were originally issued at thicknesses of 25 mm, 75 mm, or 150 mm (two 75 mm specimens stacked). Recently, however, in order to satisfy more stringent energy efficiency requirements mandated in U.S. building codes, insulation manufacturers have begun requesting CTS at thicknesses up to 225 mm (three 75 mm specimens stacked). In accordance with test guidelines in the R-value Rule, measurements for customers are usually conducted at a mean temperature of 297 K and a temperature difference of either 22.2 K or 27.8 K (40 °F or 50 °F, respectively) across the specimen [9].

3. Steady-State Thermal Transmission Properties

ASTM Practice C 1045 [10] provides a uniform calculation procedure for thermal transmission properties of materials based on measurements from steady-state one dimensional methods such as ASTM Test Method C 177. Table 1 summarizes the generalized one-dimensional equations for thermal resistance (R), conductance (C), resistivity (r), and conductivity (λ).

Table 1. Steady-State One-Dimensional Thermal Transmission Property Equations

| | Thermal Resistance $R, \text{m}^2 \cdot \text{K} \cdot \text{W}^{-1}$ | Thermal Conductance $C, \text{W} \cdot \text{m}^{-2} \cdot \text{K}^{-1}$ | Thermal Resistivity $r, \text{m} \cdot \text{K} \cdot \text{W}^{-1}$ | Thermal Conductivity $\lambda, \text{W} \cdot \text{m}^{-1} \cdot \text{K}^{-1}$ |
|---------------|--|--|---|---|
| Equation | $R = \frac{A\Delta T}{Q}$ | $C = \frac{Q}{A\Delta T}$ | $r = \frac{A\Delta T}{QL}$ | $\lambda = \frac{QL}{A\Delta T}$ |
| Relationships | $R = \frac{1}{C} = \frac{L}{\lambda}$ | $C = \frac{1}{R} = \frac{\lambda}{L}$ | $r = \frac{1}{\lambda}$ | $\lambda = \frac{1}{r}$ |

Here, Q is the time-rate of one-dimensional heat flow (in units of watts, W) through the meter area of the guarded-hot-plate apparatus, A is the meter area of the apparatus normal to the heat flow direction (in units of square meters, m^2), ΔT is the temperature difference across the specimen (in units of kelvins, K), and L is the specimen thickness (in units of meters, m). As a rule, NIST provides value assignments and uncertainty for only R and, to a lesser extent, λ for thermal insulation reference materials. Consequently, this paper presents uncertainty assessments only for thermal resistance (R) and thermal conductivity (λ).

² In 1901, Congress established the National Bureau of Standards (NBS) to support industry, commerce, scientific institutions, and all branches of government. In 1988, as part of the Omnibus Trade and Competitiveness Act, the name was changed to the National Institute of Standards and Technology (NIST) to reflect the agency’s broader mission. For historical accuracy, this report uses, where appropriate, NBS for events prior to 1988.

4. Measurement Principle

A guarded-hot-plate apparatus having appropriate plate temperature controllers can be operated in either a double sided mode or in a single-sided mode (also known as two-sided or one-sided mode, respectively). In principle, both modes of operation are covered in Test Method C 177; however, additional information on the single-sided mode is available in ASTM Practice C 1044 [11]. For completeness, this report presents both modes of operation but only the single-sided mode is examined in the uncertainty analysis.

Double-Sided Mode

Figure 1 shows the essential features of a guarded-hot-plate apparatus designed for operation near ambient temperature conditions. The plates are shown in a horizontal configuration with heat flow (Q) in the vertical (up/down) direction through the specimens. The apparatus is cylindrically symmetric about the axis indicated in Fig.1. In the traditional double-sided mode of operation, specimens of the same material having nearly the same density, size, and thickness are placed on each surface of the guarded hot plate and clamped securely by the cold plates. Ideally, the guarded hot plate and the cold plates provide constant-temperature boundary conditions to the specimen surfaces. Ideally, lateral heat flows (Q_{gap} and Q_{edge}) are reduced to negligible proportions with proper guarding and, under steady-state conditions, the apparatus provides one-dimensional heat flow (Q) normal to the meter area of

the specimen pair. Typically, a secondary guard is provided by an enclosed chamber that conditions the ambient gas (usually air) surrounding the plates to a temperature near to the mean specimen temperature (i.e., average surface temperatures of the hot and cold plates in contact with the specimens).

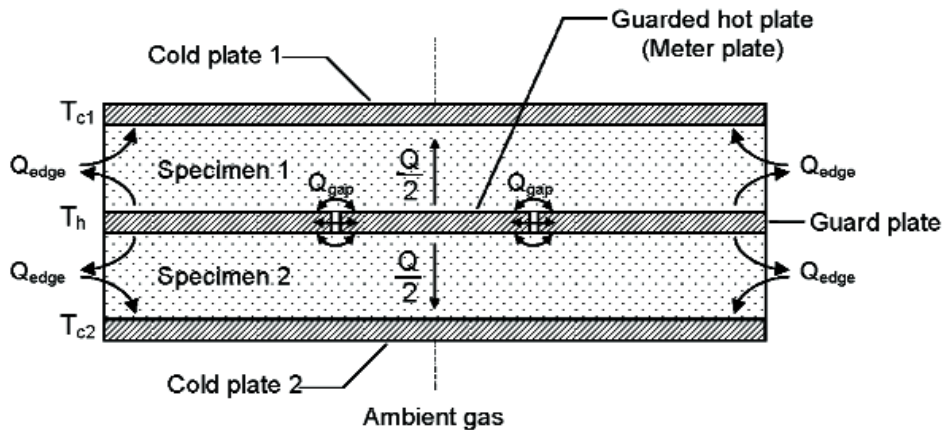
Under steady-state conditions, the operational definition [10] for the mean (apparent) thermal conductivity³ of the specimen pair (λ_{exp}) is

$$\lambda_{\text{exp}} = \frac{Q}{A[(\Delta T/L)_1 + (\Delta T/L)_2]} \quad (1)$$

where:

- Q = the time rate of one-dimensional heat flow through the meter area of both specimens and, under ideal conditions, is equal to Q_m , the electrical power input to the meter plate (W);
- A = the meter area normal to the specimen heat flow (m^2) (see Appendix A for derivation); and,
- $(\Delta T/L)_1$ = the ratio of the surface-to-surface temperature difference ($T_h - T_c$) to the thickness (L) for Specimen 1. A similar expression is used for Specimen 2.

³ The thermal transmission properties of heat insulators determined from standard test methods typically include several mechanisms of heat transfer, including conduction, radiation, and possibly convection. For that reason, some experimentalists will include the adjective “apparent” when describing thermal conductivity of thermal insulation. However, for brevity, the term thermal conductivity is used in this report.



1. Principle: $T_c < T_h$; $T_{c1} = T_{c2} = T_c$
2. Practice: $T_c < T_h$; $T_{c1} \approx T_{c2} \approx T_c$

Fig. 1. Guarded-hot-plate schematic, double-sided mode of operation—vertical heat flow.

For experimental situations where the temperature differences and the specimen thicknesses are nearly the same, respectively, Eq. (1) reduces to

$$\lambda_{\text{exp}} = \frac{QL_{\text{average}}}{2A\Delta T_{\text{average}}} \quad (2)$$

Using the relationship from Table 1, Eq. (2) can be rewritten to determine the thermal resistance of the specimen pair

$$R = \frac{2A\Delta T_{\text{average}}}{Q} \quad (3)$$

In the double-sided mode of operation, the thermal transmission properties correspond to an average temperature \bar{T} given by $\bar{T} = (T_h + T_c)/2$.

Single-Sided Mode

Figure 2 shows the essential features of a guarded-hot-plate apparatus designed for operation near ambient temperature conditions in the single-sided mode of

operation. In the single-sided mode of operation, auxiliary thermal insulation is placed between the hot plate and the auxiliary cold plate, replacing one of the specimens shown in Fig. 1.

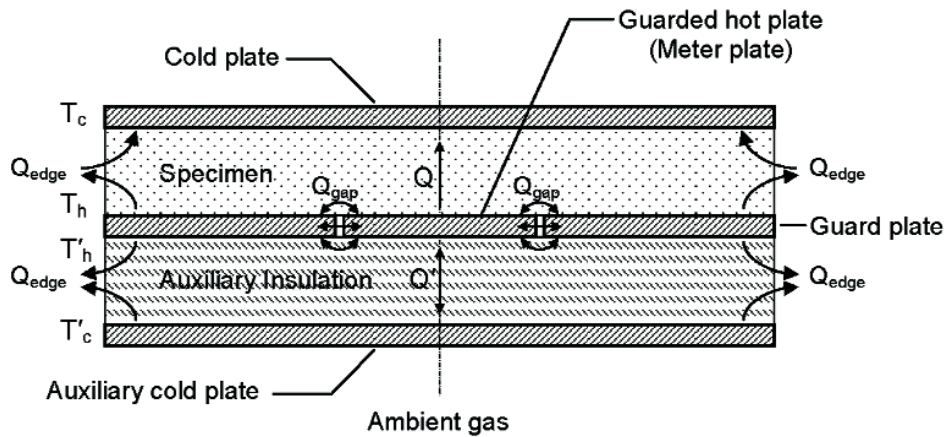
The auxiliary cold plate and the hot plate are maintained at essentially the same temperature. The heat flow (Q') through the auxiliary insulation is calculated as follows [11]:

$$Q' = C' A(T'_h - T'_c) \approx 0 \quad (4)$$

where the prime (') notation denotes a quantity associated with the auxiliary thermal insulation and C' is the thermal conductance of the auxiliary insulation. The specimen heat flow (Q) is computed in the following equation:

$$Q = Q_m - Q' \quad (5)$$

where Q_m is the power input to the meter plate. Values of Q' are typically less than 1 % of Q_m . For similar materials, Q from Eq. (5) is approximately one-half the value obtained for Q in Eq. (3) for the double-sided mode.



1. Principle: $T_c < T_h$; $T_h = T'_h = T'_c$; $Q' = 0$
2. Practice: $T_c < T_h$; $T_h \approx T'_h \approx T'_c$; $Q' \approx 0$

Fig. 2. Guarded-hot-plate schematic, single-sided mode of operation—heat flow up.

5. Apparatus

Figure 3 shows an illustration of the NIST 1016 mm Guarded-Hot-Plate apparatus. The apparatus plates are typically configured in a horizontal orientation and are enclosed by an insulated environmental chamber that can be rotated $\pm 180^\circ$. The plates are made from aluminum alloy 6061-T6. The plate surfaces in contact with the specimens are flat to within 0.05 mm and are anodized black to have a total emittance of 0.89. The hot plate is rigidly mounted on four bearing rods. Each

cold plate can translate in the vertical direction for specimen installation and is supported at its geometric center by means of a swivel ball joint that allows the plate to tilt and conform to a nonparallel rigid sample. The clamping force is transmitted axially by extension rods that are driven by a stepper motor and a worm-drive gear. A load cell measures the axial force that the plate exerts on the specimen. The cold plates are constrained in the radial direction by steel cables attached to four spring-loaded bearings that slide on the bearing rods.

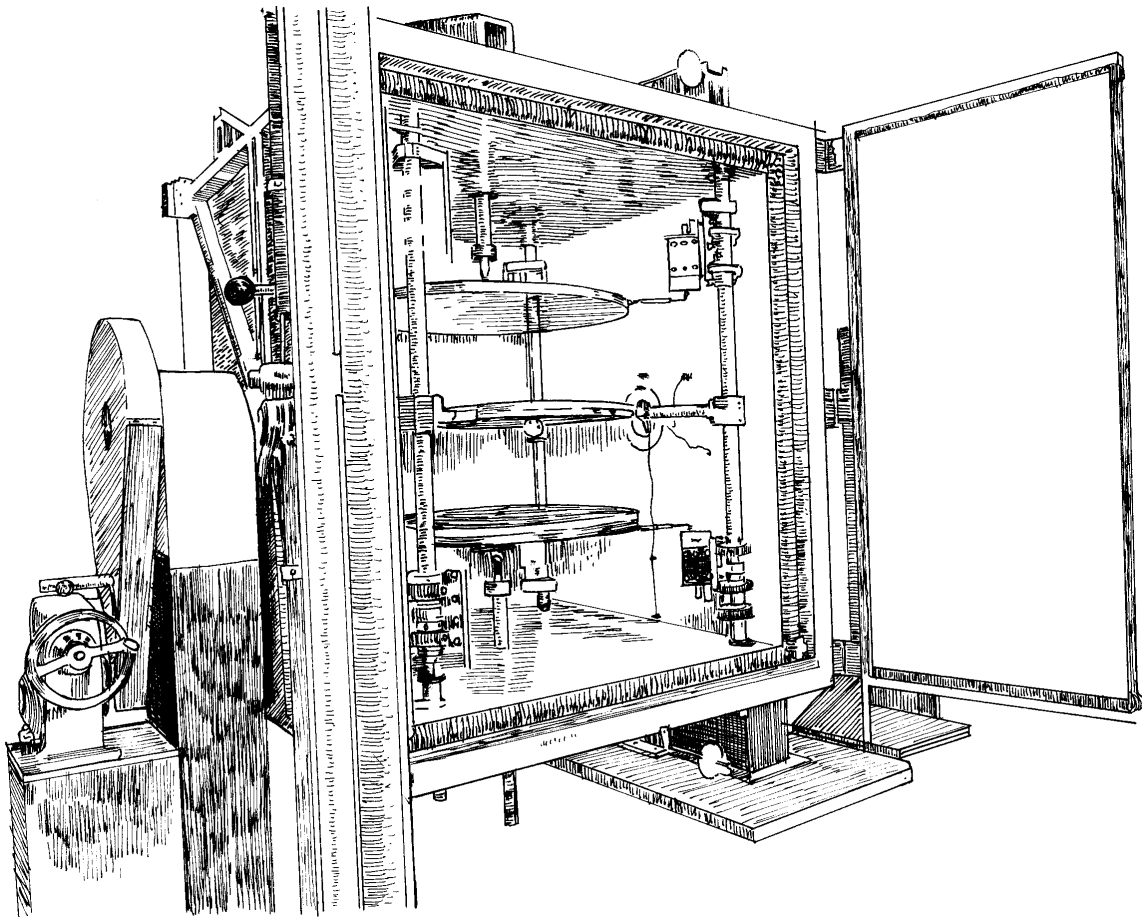


Fig. 3. NIST 1016 mm Guarded-Hot-Plate Apparatus.

Guarded Hot Plate

The 1016 mm guarded hot plate is nominally 16.1 mm thick and consists of a meter plate⁴ 405.6 mm in diameter and a co-planar, concentric guard plate with an inner diameter of 407.2 mm. The circular gap (also known as “guard gap”) that separates the meter plate and guard plate is 0.89 mm wide at the plate surface. The cross-sectional profile of the gap is diamond shaped in order to minimize lateral heat flow across the gap. The meter plate is supported within the guard plate by three stainless steel pins, equally spaced around the circumference of the meter plate, that are used to adjust the gap to a uniform width and maintain the meter plate in plane with the guard plate. Across its diameter, the meter plate is flat to within 0.025 mm.

The hot-plate heater design, described previously in detail by Hahn et al. [12], utilizes circular line-heat sources located at prescribed radii. The circular line-heat-source for the meter plate is located at a radius of $\sqrt{2}/2$ times the meter-plate radius which yields a diameter of 287 mm. This location for the heater results in a temperature profile such that the temperature at the gap is equal to the average meter-plate temperature [12]. The heating element is a thin nichrome ribbon filament network, 0.1 mm thick and 4 mm wide, electrically insulated with polyimide, having an electrical resistance at room temperature of approximately 56 Ω .

There are two circular line-heat-sources in the guard plate located at diameters of 524.7 mm and 802.2 mm. The heating elements are in metal-sheathed units, 1.59 mm in diameter, and were pressed in circular grooves cut in the surfaces of the guard plate. The grooves were subsequently filled with a high-temperature epoxy. The electrical resistances at room temperature for the inner and outer guard heaters are approximately 72 Ω and 108 Ω , respectively.

Meter-Plate Electrical Power

Figure 4 shows the electrical circuit schematic for the meter-plate power measurement which consists of a four-terminal standard resistor, nominally 0.1 Ω , in series with the meter-plate heater. A direct-current power supply (40 V) provides current (i) to the circuit which is determined by measuring the voltage drop (V_s) across the standard resistor (Fig. 4) placed in an oil bath at 25.00 $^{\circ}\text{C}$. The voltage across the meter-plate heater (V_m) is measured with voltage taps welded to the heater leads in the center of the gap (described above). The meter plate power (Q_m) is the product of V_m and i .

⁴ Terminology for the 1016 mm guarded hot plate reflects current usage in ASTM Practice C 1043.

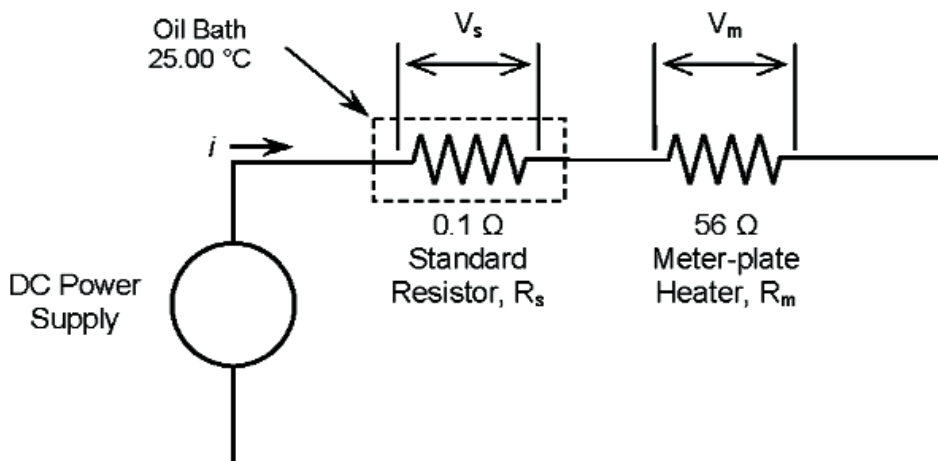


Fig. 4. Electrical schematic for meter-plate power measurement.

Cold Plates

The cold plates are fabricated from 6061-T6 aluminum and contain channels that circulate an ethylene glycol/distilled water solution. Each plate is 25.4 mm thick and consists of a 6.35 mm thick cover plate bonded with epoxy to a 19.05 mm thick base plate. The base plate has milled grooves 9.5 mm deep and 19.1 mm wide arranged in a double-spiral configuration. This arrangement forms a counter-flow heat exchanger, that is, the supply coolant flows next to the return coolant providing a uniform temperature distribution over the cold-plate surface. The temperature of each cold plate is maintained by circulating liquid coolant from a dedicated refrigerated bath regulated to within ± 0.05 K over a temperature range of -20 °C to 60 °C. The outer surfaces and edges of the cold plates are insulated with 102 mm of extruded polystyrene foam.

Environmental Chamber

The environmental chamber is a large rectangular compartment having inside dimensions of 1.40 m square by 1.60 m high supported by a horizontal axle on rotational rollers that allow the apparatus to pivot by $\pm 180^\circ$ (Fig. 3). Access to the plates and specimens is permitted by front-and-back double-doors. Air is circulated by a small fan in the chamber and is conditioned by a small cooling coil/reheat system located within the chamber.

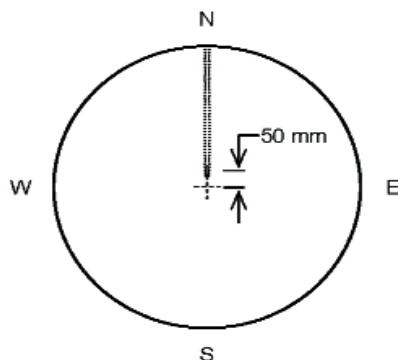


Fig. 5a. Location of cold plate PRT (top view).

The air temperature ranges from about 5 °C to 60 °C and is maintained to within ± 0.5 K by using the average of five Type T thermocouples located in the chamber.

Primary Temperature Sensors

The primary temperature sensors are small capsule platinum resistance thermometers (PRTs). The sensor construction is a strain-free platinum element supported in a gold-plated copper cylinder 3.18 mm in diameter by 9.7 mm long backfilled with helium gas and hermetically sealed. The sensors are designed for temperatures from 13 K to 533 K (-260 °C to 260 °C) and the nominal resistance is 100 Ω at 0 °C. The electrical resistance of each 4-wire PRT is measured with a digital multimeter (DMM) that is part of an automated data acquisition system.

Figure 5 shows the locations of the PRTs in the cold plates and hot plate. The cold plate PRT is inserted in a 3.26 mm diameter hole, 457 mm long, bored into the side of the cold plate (Fig. 5a). The hot plate PRT is located in the guard gap at an angle of 69° from the location where meter plate heater wires cross the guard gap (Fig. 5b) based on the theoretical temperature distribution $T(r, \theta)$ determined by Hahn et al. [12] for a similar apparatus. The sensor is fastened with a small bracket on the meter side of the gap at the mid-plane of the plate ($z = 0$) as illustrated in Fig. 5c. The radius to the center of the PRT was computed to be 199.3 mm.

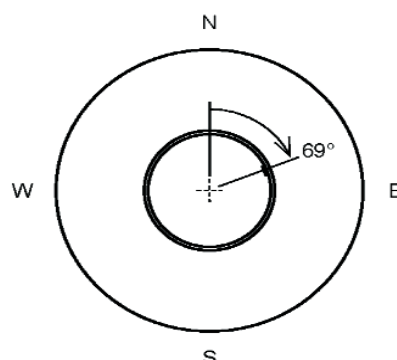


Fig. 5b. Location of hot plate PRT in guard gap on meter side of guard gap (top view).

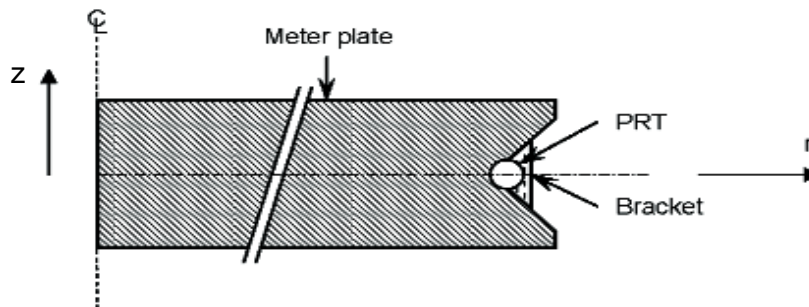


Fig. 5c. Cross-section view of PRT in guard gap (guard plate not shown).

Temperature Sensors in the Guard Gap

The temperature difference across the guard gap (ΔT_{gap}) is estimated using an eight junction (4 pairs) Type E⁵ thermopile. The thermopile was constructed from No. 30 AWG (American wire gauge) insulated thermocouple wire 0.25 mm in diameter welded in an argon atmosphere to form small bead junctions. The wire lengths were taken from spools of wire that were scanned using a large temperature gradient (i.e., a bath of liquid nitrogen) to isolate inhomogeneities in the wire. The wire passed from ambient to liquid nitrogen temperature and back to ambient; sections that gave thermoelectric voltages larger than $3 \mu\text{V}$ for EP wire and $1.7 \mu\text{V}$ for EN wire were discarded.

Figure 6 shows the angular locations for the individual junctions in the guard gap. The reference angle of 0° is the location where the meter-plate heater leads cross the gap (the same as Fig. 5b).

⁵ Type E is a letter designation for an ANSI standard base-metal thermocouple. Thermoelectric elements are designated by two letters where the second letter, P or N, denotes the positive or negative thermoelement, respectively.

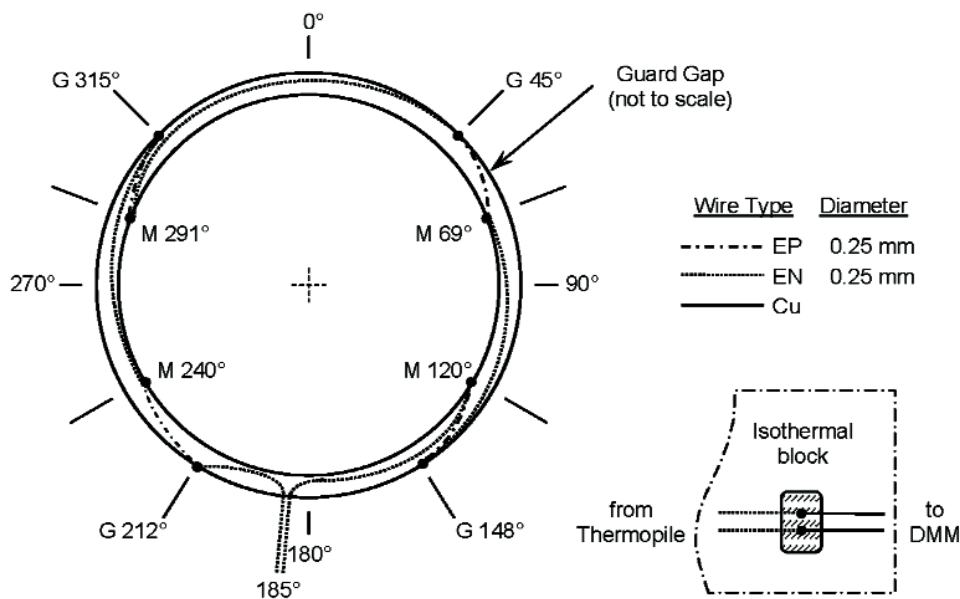


Fig. 6. Angular locations of Type E thermopile junctions in the guard gap (not to scale).

The thermocouple beads are installed in brackets with a thermally conductive epoxy and fastened, in alternating sequence, to either the meter plate or the guard plate similarly to the method used for the meter-plate PRT (Fig. 5c). Like the PRT, the junctions are located at the mid-plane of the hot plate (that is, $z = 0$ in the axial direction). The EN leads of the thermopile depart the guard gap at an angle of 185° (as shown in Fig. 6) and are connected to copper leads on an isothermal block mounted inside a small aluminum enclosure. The aluminum enclosure is located inside the environmental chamber surrounding the apparatus plates.

Temperature Control

The three heaters in the guarded hot plate are controlled by a digital proportional, integral (PI) control algorithm that operates by actively controlling the plate temperatures. In other words, the power level is not fixed at a specific level which could lead to temperature drift. Under steady-state conditions, the meter plate temperature is controlled to within $\pm 0.003 \text{ K}$.

6. Measurement Uncertainty Estimation

This section summarizes relevant uncertainty terminology consistent with current international guidelines [1-2] and presents a procedure for the estimation of measurement uncertainty based on practical experiences by analytical chemical laboratories [13]. Using this procedure, an example is given for computation of the measurement uncertainty of the low-density fibrous-glass thermal insulation issued by NIST as a CTS.

Terminology

The **combined standard uncertainty** of a measurement result, $u_c(y)$ is expressed as the positive square root of the combined variance $u_c^2(y)$:

$$u_c(y) = \sqrt{\sum_{i=1}^N c_i u^2(x_i)}. \quad (6)$$

Equation (6) is commonly referred to as the “*law of propagation of uncertainty*” or the “*root-sum-of-squares*.” The sensitivity coefficients (c_i) are equal to the partial derivative of an input quantity ($\partial f/\partial X_i$) evaluated for the input quantity equal to an input estimate ($X_i = x_i$). The corresponding term, $u(x_i)$, is the standard uncertainty associated with the input estimate x_i . The **relative combined standard uncertainty** is defined as follows (where $y \neq 0$):

$$u_{c,r}(y) = \frac{u_c(y)}{|y|}.$$

Each $u(x_i)$ is evaluated as either a **Type A** or a **Type B** standard uncertainty. Type A standard uncertainties are evaluated by statistical means. The evaluation of uncertainty by means other than a statistical analysis of a series of observations is termed a Type B evaluation [1]. Type B evaluations are usually based on scientific judgment and may include measurement data from another experiment, experience, a calibration certificate, manufacturer specification, or other means as described in Refs. [1-2]. It should be emphasized that the designations “A” and “B” apply to the two methods of evaluation, *not* the type of error. In other words, the designations “A” and “B” have nothing to do with the traditional terms “random” or “systematic.” Categorizing the evaluation of uncertainties as Type A or Type B is a matter of convenience, since both are

based on probability distributions⁶ and are combined equivalently. Thus, Eq. (6) can be expressed in simplified form as:

$$u_c = \sqrt{u_A^2 + u_B^2}. \quad (7)$$

Examples of Type A and Type B evaluations are provided in Refs. [1-2]. A typical example of a Type A evaluation entails repeated observations. Consider an input quantity X_i determined from n independent observations obtained under the same conditions. In this case, the input estimate x_i is the sample mean determined from

$$x_i = \bar{X}_i = \frac{1}{n} \sum_{k=1}^n X_{i,k}.$$

The standard uncertainty, $u(x_i)$ associated with x_i is the estimated standard deviation of the sample mean (where s is the standard deviation of n observations):

$$u(x_i) = s(\bar{X}_i) = \frac{s}{\sqrt{n}}. \quad (8)$$

The **expanded uncertainty**, U , is obtained by multiplying the combined standard uncertainty, $u_c(y)$, by a coverage factor, k when an additional level of uncertainty is required that provides an interval (similar to a confidence interval, for example):

$$U = k u_c(y) = \sqrt{\sum c_i^2 u^2(x_i)_A + \sum c_i^2 u^2(x_i)_B}. \quad (9)$$

The value of k is chosen based on the desired level of confidence to be associated with the interval defined by U and typically ranges from 2 to 3. Under a wide variety of circumstances, a coverage factor of $k = 2$ defines an interval having a level of confidence of about 95 % and $k = 3$ defines an interval having a level of confidence greater than 99 %. At NIST, a coverage factor of $k = 2$ is used, by convention [1]. The **relative expanded uncertainty** is defined as follows (where $y \neq 0$):

$$U_r = \frac{U}{|y|}.$$

⁶ Note that the probability distribution for a Type B evaluation, in contrast to a Type A evaluation, is assumed based on the judgment of the experimenter.

For Type A evaluations, the *degrees of freedom*, ν , is equal to $n - 1$ for the simple case given in Eq. (8). For the case when u_c is the sum of two or more variance components, an *effective* degrees of freedom is obtained from the Welch-Satterthwaite formula as described in Refs. [1-2]. For Type B evaluations, ν is assumed to be infinity. As will be shown later in this report, the Type B evaluation is the dominant component of uncertainty. Therefore, values for ν are not necessary and are not ultimately used in determination of the coverage factor, k .

Procedure

The EURACHEM/CITAC Guide [13] provides a practical guide for the estimation of measurement uncertainty based on the approach presented in the GUM [2]. Although developed primarily for analytical chemical measurements, the concepts of the EURACHEM/CITAC Guide are applicable to other fields. The primary steps are summarized below:

- Specification of the mathematical process (measurement) model—clear and unambiguous statement of the measurand, i.e., $Y = f(X_1, X_2, \dots, X_N)$.
- Identification of uncertainty sources—a comprehensive (although perhaps not exhaustive) list of relevant uncertainty sources. A cause-and-effect diagram is a useful means for assembling this list.
- Quantification of the components of the uncertainty sources—a detailed evaluation of the component uncertainties using Type A and/or Type B evaluations described above (for example, Eq. (8)) or in the GUM.
- Calculation of the combined standard uncertainty—propagate the component uncertainties using the “law of propagation uncertainty” given in Eq. (6).
- Calculation of the expanded uncertainty—using a coverage factor of $k = 2$, compute an interval for the expanded uncertainty given in Eq. (9).

7. Mathematical Process Model

Mathematical process models are specified for thermal conductivity (λ) and thermal resistance (R) as determined using the single-sided mode of operation (Fig. 2). For λ , the mathematical process model is given by

$$\lambda_{\text{exp}} = \frac{QL}{A(\Delta T)} = \frac{(Q_m - \Delta Q)L}{A(T_h - T_c)} \quad (10)$$

$$= \frac{(Q_m - Q_{\text{gap}} - Q' - Q_\epsilon)L}{A(T_h - T_c)}$$

where:

- Q_m = power input (W) to the meter plate heater;
- ΔQ = parasitic heat transfer (W) from the meter area (defined more specifically as Q_{gap} , Q' , and Q_ϵ);
- Q_{gap} = lateral heat flow (W) across the guard gap (i.e., the airspace separation between the meter plate and guard plate shown in Fig. 2);
- Q' = heat flow (W) through the meter section of the auxiliary insulation (Fig. 2);
- Q_ϵ = error due to edge heat transfer (W) (i.e., from Q_{edge} shown in Fig. 2);
- L = *in-situ* thickness of the specimen during testing (m);
- A = meter area normal to Q (m²);
- ΔT = specimen temperature difference (K);
- T_h = temperature of hot plate (K); and,
- T_c = temperature of cold plate (K).

For R , the mathematical process model is given by

$$R = \frac{A(\Delta T)}{Q} = \frac{A(T_h - T_c)}{Q_m - \Delta Q} \quad (11)$$

$$= \frac{A(T_h - T_c)}{Q_m - Q_{\text{gap}} - Q' - Q_\epsilon}$$

One of the major differences between Eqs. (10) and (11) is the absence of the term for specimen thickness (L) in Eq. (11). With regards to sign convention for heat flow (Q), heat gain to the meter area is assumed to be positive (+) and heat loss is assumed to be negative (-).

8. Sources of Uncertainty

Figure 7 shows a cause-and-effect diagram that has been developed for λ_{exp} from Eq. (10). The cause-and-effect diagram is a hierarchical structure that identifies the main sources (shown as arrows directly affecting λ_{exp}) and secondary factors (shown as arrows

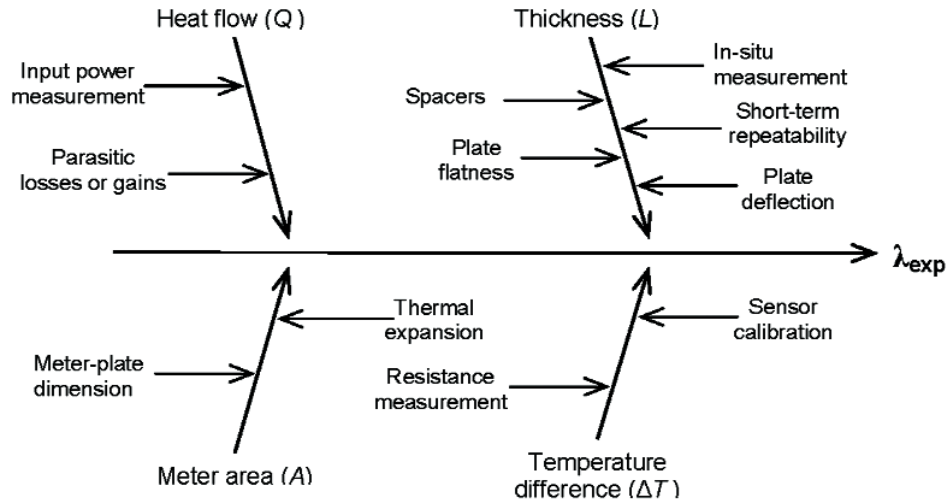


Fig. 7. Cause-and-effect chart for λ_{exp} (2 levels of contributory effects).

affecting Q , L , A , and ΔT) of contributory uncertainty. Tertiary (and additional hierarchical) factors of contributory uncertainty are not shown in Fig. 7. In general, the uncertainty sources in Fig. 7 can be grouped in one of three major metrology categories—dimensional metrology for meter area (A) and thickness (L); thermal metrology for temperature (T); and, electrical metrology for voltage (V) and resistance (Ω) measurements. The analysis of parasitic heat losses and/or gains (ΔQ) requires either additional heat-transfer analyses or experiments (or both).

From Fig. 7, a comprehensive, but not exhaustive, list of uncertainty sources is developed as shown in Table 2. This particular list could be applied to other apparatus but is most applicable to the NIST 1016 mm Guarded-Hot-Plate apparatus for single-sided measurements of low-density fibrous-glass blanket thermal insulation. Other materials, mode of operation, apparatus, etc. may require a (slightly) different listing of sources (see, for example, the uncertainty analysis for NIST SRM 1450c [3]).

Table 2. List of Uncertainty Sources for λ for the NIST 1016 mm Guarded-Hot-Plate Apparatus

| | |
|--|---|
| 1) Meter area (A) a) Plate dimensions b) Thermal expansion effects | i) Digital multimeter (DMM) uncertainty ii) PRT regression uncertainty in fit for calibration data |
| 2) Thickness (L) a) In-situ linear position measurement system i) Multiple observations ii) System uncertainty b) Dimensions of fused-quartz spacers i) Repeated observations ii) Caliper uncertainty c) Short-term repeatability d) Plate flatness i) Repeated observations ii) Coordinate measuring machine (CMM) uncertainty e) Plate deflection under axial loading of cold plate | b) Calibration of PRTs c) Miscellaneous sources (not shown in Fig. 7) i) Contact resistance ii) Sampling of planar plate temperature iii) Axial temperature variations |
| 3) Temperature difference (ΔT) a) Measurement (T_h, T_c) | 4) Heat flow (Q) a) DC power measurement (Q_m) i) Standard resistor calibration ii) Standard resistor drift iii) PRT power input iv) Voltage measurement b) Parasitic heat flows (ΔQ) i) Guard-gap (Q_{gap}) ii) Auxiliary insulation (Q') iii) Edge effects (Q_ϵ) |

The list of contributory sources of uncertainty for R is the same as the list given in Table 2 except the con-

tributory source for L would be omitted, as shown in Eq. (11).

9. Quantification of Uncertainty Components

Analysis of the standard uncertainties for meter area (A), thickness (L), temperature difference (ΔT), and power (Q) are presented in this section. A useful approach that is followed in this report is to treat each uncertainty component separately and evaluate the uncertainty component as either a Type A or Type B standard uncertainty [1-2]. The example presented here is for specimens of low-density fibrous-glass thermal insulation taken from the CTS lot of reference material in thicknesses of 25.4 mm, 76.2 mm, 152.4 mm, 228.6 mm. The guarded-hot-plate measurements were conducted at a mean temperature of 297 K and a temperature difference of 22.2 K. The apparatus was operated in the single-sided mode of operation utilizing a specimen of expanded polystyrene foam having a nominal thickness of 100 mm as the auxiliary insulation (Fig. 2).

Meter Area (A)

The meter area is the mathematical area through which the heat input to the meter plate (Q) flows normal to the heat-flow direction under ideal guarding conditions (i.e., $Q_{gap} = Q_e \equiv 0$) into the specimen. It is important to emphasize that the meter area is not the same as the area of the meter plate (shown in Figs. 1 and 2). The circular meter area was calculated from Eq. (12) below (see Appendix A for derivation):

$$A = \frac{\pi}{2} (r_o^2 + r_i^2) (1 + \alpha \Delta T_{mp})^2 \quad (12)$$

where:

- r_o = outer radius of meter plate (m);
- r_i = inner radius of guard plate (m);
- α = coefficient of thermal expansion of aluminum (alloy 6061-T6) (K^{-1}); and,
- ΔT_{mp} = temperature difference of the meter plate from ambient (K) = $T_h - 20$ °C.

The application of Eq. (6) to Eq. (12) yields

$$u_c(A) = \sqrt{c_{r_o}^2 u^2(r_o) + c_{r_i}^2 u^2(r_i) + c_\alpha^2 u^2(\alpha) + c_{\Delta T_{mp}}^2 u^2(\Delta T_{mp})}$$

with

$$\begin{aligned} c_{r_o} &= \partial A / \partial r_o = \pi r_o (1 + \alpha \Delta T_{mp})^2 \\ c_{r_i} &= \partial A / \partial r_i = \pi r_i (1 + \alpha \Delta T_{mp})^2 \\ c_\alpha &= \partial A / \partial \alpha = \pi \Delta T_{mp} (r_o^2 + r_i^2) (1 + \alpha \Delta T_{mp}) \\ c_{\Delta T_{mp}} &= \partial A / \partial (\Delta T_{mp}) = \pi \alpha (r_o^2 + r_i^2) (1 + \alpha \Delta T_{mp}) \end{aligned}$$

Plate Dimensions: The design gap dimensions [5] for the meter plate and the guard plate diameters are 405.64 mm (15.970 in) and 407.42 mm (16.040 in), respectively. In 1994, as part of an extensive sensor calibration check, the meter plate was separated and removed from the guard plate. Using a coordinate measuring machine, the roundness of the meter plate was checked at six locations at the periphery and the diameter was determined to be 405.67 mm (15.971 in). During re-assembly, a uniform gap width of 0.89 mm (0.035 in) was re-established using three pin gages spaced at equiangular intervals between the meter plate and guard plate. The uncertainty of the pin gages was + 0.005 mm / - 0.000 mm. Based on these check measurements, the input values for r_o and r_i , were determined to be 0.20282 m and 0.20371 m, respectively, and the standard uncertainty for both input values was taken to be 0.0254 mm (0.001 in.).

Thermal Expansion: For α , an input value of $23.6 \times 10^{-6} K^{-1}$ was taken from handbook data for aluminum alloy 6061-T6. The standard uncertainty for the value of α was assumed to be 10 % (that is, $2.36 \times 10^{-6} K^{-1}$). For tests conducted at a mean temperature of 297 K and a specimen temperature difference of 22.2 K, the meter plate temperature (T_h) was maintained at 308 K (35 °C, 95 °F); thus, ΔT_{mp} was equal to + 15 K. The standard uncertainty for ΔT_{mp} was determined to be 0.086 K (and will be discussed later in the section on ΔT uncertainty).

$u_c(A)$: Substituting the above input estimates into Eq. (12), yields a meter area (A) of 0.12989 m². For $u_c(A)$, the input estimates (x_i), sensitivity coefficients (c_i), standard uncertainties ($u(x_i)$), and evaluation method (Type A or B) are summarized in Table 3. The last column in Table 3 provides values for $c_i \cdot u(x_i)$ to assess the uncertainty contribution for each input X_i . The combined standard uncertainty $u_c(A)$ and relative standard uncertainty $u_{c,r}(A)$ were determined to be $2.4732 \times 10^{-5} m^2$ and 0.019 %, respectively. This estimate for $u_c(A)$ is quite small near ambient temperature but increases as T_h departs from ambient conditions.

Table 3. Summary of Standard Uncertainty Components for Meter Area (A)

| X_i | x_i | c_i | $u(x_i)$ | Type | $c_i \cdot u(x_i)$ |
|-----------------|--------------------------------------|---|--------------------------------------|------|------------------------------------|
| r_o | 0.20282 m | 0.63763 m | 0.0000254 m | B | $16.20 \times 10^{-6} \text{ m}^2$ |
| r_i | 0.20371 m | 0.64042 m | 0.0000254 m | B | $16.27 \times 10^{-6} \text{ m}^2$ |
| α | $23.6 \times 10^{-6} \text{ K}^{-1}$ | $3.8953 \text{ m}^2 \cdot \text{K}$ | $2.36 \times 10^{-6} \text{ K}^{-1}$ | B | $9.19 \times 10^{-6} \text{ m}^2$ |
| ΔT_{mp} | 15 K | $6.13 \times 10^{-6} \text{ m}^2 \cdot \text{K}^{-1}$ | 0.086 K | B | $0.53 \times 10^{-6} \text{ m}^2$ |

Thickness (L)

In the single-sided mode of operation, the in-situ thickness of the specimen (Fig. 2) is monitored during a test by averaging four linear position transducers attached to the periphery of the cold plate at approximate 90° intervals.⁷ Each device consists of a digital readout and a slider that translates in close proximity to (but not in contact with) a 580 mm precision tape scale bonded to a precision ground plate of a low thermal expansion iron-nickel (FeNi36) alloy. In operation, the slider is excited with a pair of oscillating voltages which are out-of-phase by 90° . The electrical windings on the scale are inductively coupled with the slider and the resulting output signal from the scale is resolved and processed by the digital readout. As the slider follows the axial movement of the cold plate, the corresponding output signal represents the linear distance between the translating cold plate and the stationary hot plate.

The digital readouts are reset by placing a set of four fused-quartz spacers of known thickness between the cold plate and hot plate. Fused-quartz tubing was selected because of its low coefficient of thermal expansion ($5.5 \times 10^{-7} \text{ K}^{-1}$) and high elastic modulus (72 GPa). The tubes have nominal inner and outer diameters of 22 mm and 25 mm, respectively. Loose-fill thermal insulation was placed in the tubes to suppress any convective heat transfer. Because the fibrous-glass blanket CTS is compressible, the plate separation is maintained during a test by four fused-quartz spacers placed at the periphery of the specimen at the same angular intervals as the four linear position transducers described above. Four sets of spacers having lengths of 25.4 mm, 76.2 mm, 152.4 mm, and 228.6 mm cover the thickness range of interest for fibrous-glass blanket CTS.

The combined standard uncertainty for L is given by

$$u_c(L) = \sqrt{u^2(L_1) + u^2(L_2) + u^2(L_3) + u^2(L_4) + u^2(L_5)} \quad (13)$$

⁷ For a two-sided test (Fig. 1), eight linear positioning devices (four for each specimen) determine the in-situ thickness of the specimen pair.

where the sensitivity coefficients are equal to unity ($c_{L_i} = 1$) and the contributory uncertainties, identified in Fig. 7, are

- $u(L_1)$ = standard uncertainty of the in-situ linear position measurement (m);
- $u(L_2)$ = standard uncertainty of the fused-quartz spacers (m);
- $u(L_3)$ = standard uncertainty of the repeatability of the linear position measurement (m);
- $u(L_4)$ = standard uncertainty of the plate flatness (m); and,
- $u(L_5)$ = standard uncertainty of the cold plate deflection under axial loading (m).

The contributory uncertainties $u(L_i)$ are discussed in detail below.

$u(L_1)$ —*In-situ Measurement*: During a test, the digital readouts are recorded manually and the estimate for $x(L_1)$ is determined from the sample mean of the four observations. Two contributory effects comprise $u(L_1)$: 1) multiple observations (Type A evaluation); and, 2) the measurement system uncertainty (Type B evaluation). Thermal expansion effects of the linear tape scales were neglected because the iron-nickel (36 %) alloy has a low coefficient of thermal expansion and the tests are conducted near ambient conditions of 297 K. Equation (8) is applied to evaluate the Type A standard uncertainty where s is the standard deviation of the four transducers ($n = 4$). The Type B evaluation is the uncertainty specification stated by manufacturer ($k = 1$) of 0.005 mm. Application of Eq. (7) yields

$$u_c(L_1) = \sqrt{u_A^2 + (5.0 \times 10^{-6})^2}$$

where u_A varies for a particular test. Estimates for $u(L_1)_A$ for a test thickness of 25.4 mm are summarized at the end of this section (see Table 5).

$u(L_2)$ —*Spacers*: Two contributory effects comprise $u(L_2)$: 1) multiple length observations (Type A evaluation); and, 2) caliper uncertainty (Type B evaluation). Thermal expansion effects were neglected because fused quartz has a low coefficient of thermal expansion ($5.5 \times 10^{-7} \text{ K}^{-1}$) and the tests were conducted near ambient conditions of 297 K. Deformation of the spacers under load was also neglected because of the cross-sectional area of tubing and the relatively high value for elastic modulus. The length of each spacer was measured under ambient conditions with digital calipers and $x(L_2)$ was determined from the sample mean of four observations. Equation (8) is applied to evaluate the Type A standard uncertainty where s is the standard deviation of the four observations ($n = 4$). The Type B evaluation assumes a uniform distribution with an interval of $2a$ [2]; thus, $u_B = a/\sqrt{3}$ where a is the smallest length interval of the caliper. The estimates for u_A and u_B vary for each set of spacers and for the type of measurement calipers, respectively. Estimates for $u(L_2)_{A,B}$ for a test thickness of 25.4 mm are summarized at the end of this section (see Table 5).

$u(L_3)$ —*Repeatability*: The short-term repeatability of the linear position transducers was determined from a series of replicate measurements. For these measurements, the digital readouts were initially set to the length values of each set of fused-quartz spacers placed between the cold plate and hot plate. The cold plate was lifted from the spacers and subsequently lowered in contact with the spacers five times to check within-day variation. The procedure was repeated for four consecutive days to check the day-to-day variation (20 observations total).

The standard uncertainty for $u(L_3)$ was determined using the Type A evaluation given in Eq. (14) [14]

$$u(L_3) = \sqrt{s_a^2 + \left(\frac{r-1}{r}\right)s_d^2}; \quad (14)$$

where s_a is the standard deviation of the daily averages (between-day variation), s_d is the (pooled) within-day standard deviation, and r is number of replicates per day ($r = 5$). Table 4 summarizes replication statistics

Table 4. Summary of Replication Statistics for Uncertainty Component $u(L_3)$

| Nominal L (mm) | Day | Replicates | Within-day Average (m) | Within-day Standard Deviation (m) | S_a (m) | S_d (m) | $u(L_3)$ (m) |
|------------------------|-----|------------|------------------------------|---|-----------------------|-----------------------|-----------------------|
| 25.4 | 1 | 5 | 0.0254051 | 3.96×10^{-6} | 5.12×10^{-6} | 4.24×10^{-6} | 6.37×10^{-6} |
| | 2 | 5 | 0.0254144 | 4.28×10^{-6} | | | |
| | 3 | 5 | 0.0254156 | 3.29×10^{-6} | | | |
| | 4 | 5 | 0.0254159 | 5.20×10^{-6} | | | |
| 76.2 | 1 | 5 | 0.0762217 | 0.70×10^{-6} | 6.69×10^{-6} | 2.25×10^{-6} | 6.98×10^{-6} |
| | 2 | 5 | 0.0762325 | 1.93×10^{-6} | | | |
| | 3 | 5 | 0.0762376 | 1.38×10^{-6} | | | |
| | 4 | 5 | 0.0762325 | 3.77×10^{-6} | | | |
| 152.4 | 1 | 5 | 0.152405 | 3.68×10^{-6} | 2.48×10^{-6} | 2.95×10^{-6} | 3.62×10^{-6} |
| | 2 | 5 | 0.152410 | 0.70×10^{-6} | | | |
| | 3 | 5 | 0.152411 | 3.45×10^{-6} | | | |
| | 4 | 5 | 0.152409 | 2.98×10^{-6} | | | |
| 228.6 | 1 | 5 | 0.228578 | 10.79×10^{-6} | 6.28×10^{-6} | 6.88×10^{-6} | 8.79×10^{-6} |
| | 2 | 5 | 0.228569 | 7.64×10^{-6} | | | |
| | 3 | 5 | 0.228582 | 2.75×10^{-6} | | | |
| | 4 | 5 | 0.228571 | 2.63×10^{-6} | | | |

for nominal specimen thicknesses of 25.4 mm, 76.2 mm, 152.4 mm, and 228.6 mm. Values for within-day average and within-day standard deviation for the 5 replicates are given in columns 4 and 5, respectively, and values for s_a , s_d , and $u(L_3)$ for each nominal level of thickness are summarized in the last three columns of Table 4. Note that values of $u(L_3)$ in Table 4 do not appear to be correlated with L . The degrees of freedom (ν) for Eq. (14) were determined from the Welch-Satterthwaite formula [1] and the value is summarized at the end of this section (see Table 5).

$u(L_4)$ —*Plate Flatness*: Two contributory effects comprise $u(L_4)$: 1) multiple thickness observations (Type A evaluation); and, 2) coordinate measuring machine (CMM) uncertainty (Type B evaluation). As discussed above, the meter plate dimensions were checked with a CMM in 1994. The thickness of the plate was measured at 32 different locations using a CMM and the estimate for $x(L_4)$ was determined from the sample mean of 32 observations. The standard deviation (s) was 0.0131 mm and, thus, the relative flatness over the meter plate is $(0.013 \text{ mm})/(406.4 \text{ mm}) = 0.003 \%$. It is interesting to note that the flatness specification given in C177-04 is 0.025 % [7]. Application of Eq. (8) to evaluate the Type A standard uncertainty yields:

$$u(L_4)_A = 1.31 \times 10^{-5} \text{ m} / \sqrt{32} = 2.32 \times 10^{-6} \text{ m}.$$

The Type B evaluation is the uncertainty specification ($k = 1$) for the CMM of 0.0051 mm. Because the cold plate was fabricated with the same machine finish as the meter plate, the cold plate flatness is assumed to be nearly the same as the meter plate. In this case, Eq. (7) becomes:

$$u_c(L_4) = \sqrt{2(u_A^2 + u_B^2)}.$$

Substituting the values for the Type A and Type B evaluations given above yields a standard uncertainty for L_4 of 0.0079 mm. The value of $u(L_4)$ (0.0079 mm) is apparatus dependent and, thus, is fixed for all values of specimen thickness.

$u(L_5)$ —*Cold Plate Deflection*: The potential deflection of the (large) cold plate under a mechanical load is evaluated as a Type B uncertainty using classical stress and strain formulae developed for flat plates. As will be discussed below, this approach is an approximation. Recall that the clamping force on the specimen and auxiliary insulation is transmitted axially by extension rods (Fig. 3). The axial force is applied over a circular

area at the center of each plate and is assumed to be uniformly distributed through a ball joint connection between the plate and extension rod. In the single-sided mode of operation, the auxiliary insulation is a rigid specimen of expanded polystyrene foam which supports the hot plate (Fig. 2). For a uniform load over a concentric circular area of radius r , the maximum deflection y_{max} at the center of the cold plate is given by the following formula from Ref. [15]. In this case, simple edge support is assumed because the test specimen is compressible and the plate separation is maintained by edge spacers.

$$u(L_5) = y_{max} = \frac{3W(m^2 - 1)}{16\pi Em^2 t^3} \left[\frac{(12m + 4)a^2}{m + 1} - 4r^2 \ln \frac{a}{r} - \frac{(7m + 3)r^2}{m + 1} \right] \quad (15)$$

where:

- W = total applied load (N);
- m = reciprocal of Poisson's ratio (dimensionless);
- E = modulus of elasticity ($\text{N} \cdot \text{m}^{-2}$);
- t = thickness of the plate (m); and,
- a = radius of the plate (m).

Based on load cell measurements, a conservative estimate for the net applied force (W) for the cold plate was assumed to be 356 N (80 lbf). The plate is 1.016 m in diameter and 0.0254 m thick and is fabricated from aluminum alloy 6061-T6. The values for m , E , and r were taken to be $(0.33)^{-1} = 3.0$, $6.9 \times 10^7 \text{ kPa}$ ($10 \times 10^6 \text{ lb}_f \cdot \text{in}^{-2}$), and 0.305 m, respectively. Substituting into Eq. (15) yields a value of 0.031 mm for y_{max} , which is the dominant component of the thickness uncertainty and is essentially fixed for each level of specimen thickness (for constant loading).

In general, the uncertainty due to plate deflection depends on the apparatus plate design (i.e., dimensions and material), the rigidity of the test specimen, and the magnitude and application of the load applied. The major limitations for this assessment approach are:

- The cold plate is not simply supported as assumed in Eq. (15). The plate is actually constrained by the fused-quartz spacers at four locations around the periphery of the plate.
- The cold plate is not a solid plate. As discussed above, the cold plate is actually a composite construction to allow the flow of coolant internally within the plate.

$u_c(L)$: Table 5 summarizes the sources, sensitivity coefficients (c_i), uncertainty components $u(L_i)$, and the evaluation method (Type A or B) for a thickness of 25.4 mm ($L_{25.4}$). As described above, the component uncertainties are either test dependent ($u(L_1)$), spacer dependent ($u(L_2)$), process dependent ($u(L_3)$), or apparatus dependent ($u(L_4)$) and $u(L_5)$). The final two components are essentially fixed for all thicknesses. Consequently, only the first three rows of Table 5 are applicable for 25.4 mm thick specimens. Application of Eq. (13) yields a combined standard uncertainty for $L_{25.4}$ of 0.038 mm ($u_{c,r}(L) = 0.15\%$). It is interesting to note that C 177-04 requires that the specimen thickness be determined to within 0.5 % [7].

Table 6 summarizes $u(L_i)$, $u_c(L)$, and $u_{c,r}(L)$ for specimen thicknesses of 25.4 mm, 76.2 mm, 152.4 mm, and 228.6 mm. As discussed above, the dominant component for all levels of thickness is $u(L_5)$, the uncertainty due to potential deflection of the cold plate. As a result, the variation of $u_c(L)$ is small over the range of thicknesses. One should note that the values given in Table 6 are valid only for the apparatus described herein. Other guarded-hot-plate apparatus would have different sources and values for the thickness uncertainty components. For example, the uncertainty due to plate flatness could be much larger if proper attention is not given to the plate design and fabrication.

Table 5. Summary of Standard Uncertainty Components for 25.4 mm Thickness ($L_{25.4}$)

| $u(x_i)$ | Source | c_i | Value of $u(L_i)$ | Type |
|----------|--|-------|--|---|
| $u(L_1)$ | In-situ measurement multiple observations system uncertainty | 1 | 20×10^{-6} m 19×10^{-6} m 5.0×10^{-6} m | B A (degrees of freedom = 3) B (equipment specification, $k = 1$) |
| $u(L_2)$ | Spacers (nominal 25.4) repeated observations caliper uncertainty | 1 | 1.9×10^{-6} m 1.1×10^{-6} m 1.5×10^{-6} m | B A (degrees of freedom = 12) B ($a/\sqrt{3}$ where $a = 2.54 \times 10^{-6}$ m) |
| $u(L_3)$ | Short-term repeatability | 1 | 6.4×10^{-6} m | A (degrees of freedom = 6.8) |
| $u(L_4)$ | Plate flatness repeated observations CMM uncertainty | 1 | 7.9×10^{-6} m 2.3×10^{-6} m 5.1×10^{-6} m | B A (degrees of freedom = 31) B (equipment specification, $k = 1$) |
| $u(L_5)$ | Plate deflection under load | 1 | 31×10^{-6} m | B (calculation [15]) |

Table 6. Combined Standard Uncertainty $u_c(L)$

| (L) (mm) | $u(L_1)$ (m) | $u(L_2)$ (m) | $u(L_3)$ (m) | $u(L_4)$ (m) | $u(L_5)$ (m) | $u_c(L)$ (mm) | $u_{c,r}(L)$ (%) |
|---------------|----------------------|----------------------|----------------------|----------------------|---------------------|------------------|---------------------|
| 25.4 | 20×10^{-6} | 1.9×10^{-6} | 6.4×10^{-6} | 7.9×10^{-6} | 31×10^{-6} | 0.038 | 0.15 |
| 76.2 | 12×10^{-6} | 2.4×10^{-6} | 7.0×10^{-6} | 7.9×10^{-6} | 31×10^{-6} | 0.035 | 0.05 |
| 152.4 | 12×10^{-6} | 7.7×10^{-6} | 3.6×10^{-6} | 7.9×10^{-6} | 31×10^{-6} | 0.035 | 0.02 |
| 228.6 | 9.6×10^{-6} | 9.5×10^{-6} | 8.8×10^{-6} | 7.9×10^{-6} | 31×10^{-6} | 0.035 | 0.02 |

Temperature Difference (ΔT)

As discussed above, the *primary* plate temperatures (Figs. 1-2) are monitored during a test by computing temporal averages of three small capsule platinum resistance thermometers (PRTs) ($n = 240$ observations taken over a steady-state interval of 4 h). The uncertainty sources $u(T)$ for the primary temperature sensors are discussed in detail below. *Secondary* temperature sensors such as thermocouples and thermistors located in the plates, and their corresponding uncertainties, are not discussed because these sensors are not input quantities in the mathematical process models given in Eqs. (10) and (11).

$u(T_1)$ —*Measurement*: During a typical CTS test (4 h in duration), the electrical resistances of the PRTs are recorded every minute by an automated data acquisition system ($n = 240$). Two major contributory effects comprise $u(T_1)$: 1) regression equation coefficients (Type A evaluation); and, 2) the measurement system uncertainty (Type B evaluation). (The standard uncertainty for repeated observations of ΔT (Type A evaluation) was less than 0.0002 K and was neglected in further analyses.)

- 1) For each PRT, individual observations in ohms (Ω) were converted to temperature using a curve fit to the calibration data (discussed below). The curve-fits were obtained using a statistical plotting package from NIST. The residual standard deviation for the fit of each set of calibration data was “pooled” and the resulting standard uncertainty is 0.0052 K. The degrees of freedom from the regression analyses were aggregated for a value of 15.
- 2) The Type B standard uncertainty for the resistance measurement assumes a uniform distribution with an interval $2a$ [2] where a was determined from the specification of the manufacturer for the digital multimeter (DMM). For $a = 0.039 \Omega$ at the 300 Ω DMM range, $u_B = a/\sqrt{3} = 0.022 \Omega$. This standard uncertainty in ohms was propagated using the above curve fit to yield a standard uncertainty for temperature of 0.058 K.

$u(T_2)$ —*Calibration*: The PRTs were calibrated by the NIST Thermometry Group by comparison with a standard platinum resistance thermometer in stirred liquid

baths. The thermometer was inserted into a test tube partially filled with mineral oil which, in turn, was placed in the calibration bath. In 1981, the thermometers were calibrated at the water triple point, 10 °C, 20 °C, 30 °C, 40 °C, and 50 °C [4]. In 1993, the thermometers were removed from the apparatus and recalibrated over an extended temperature range at -40 °C, 0 °C, 40 °C, 80 °C, and 120 °C. All temperatures in the 1993 calibration were based on the International Temperature Scale of 1990 (ITS-90). Based on the expanded uncertainty ($k = 2$) for the calibration bath temperatures of 0.01 K (Type B evaluation), the standard uncertainty was 0.005 K ($k = 1$). Recently, the cold plate PRTs have been removed from their respective plates and again submitted for calibration by the NIST Thermometry Group. These results will be updated when the most recent calibration and analysis are completed.

$u(T_3)$ —*Other Small or Negligible Contributors*: Several small or negligible contributory effects include the following: 1) PRT self heating/contact resistance; 2) sampling of temperatures in the meter area (r, θ); and, 3) temperature variations in the axial (z) direction (Fig. 5c). It is difficult to quantify the uncertainties of these contributors by separate experiments and, in some cases, the uncertainties are based on theoretical calculations or experimenter judgment. Hence, in all cases, the uncertainties are Type B evaluations.

- 1) *PRT self-heating/contact resistance*—The PRT excitation current is 1 mA which, for a nominal 100 Ω PRT, dissipates about 0.0001 W. For the meter plate PRT, a thin layer of thermally conductive silicone paste has been applied around the sensor to improve thermal contact (Fig. 5c). For the cold plate PRTs, the thermal conductance of the metal-to-air-to-metal interface between sensor and plate is estimated to be $0.058 \text{ W} \cdot \text{K}^{-1}$. Thus, the temperature rise ($0.0001 \text{ W}/0.058 \text{ W} \cdot \text{K}^{-1}$) is 0.0017 K.
- 2) *Sampling (planar)*—Rennex [4] and Siu [16] empirically determined the temperature profiles of different NIST meter plates utilizing independent thermopile constructions. In each experiment, the thermopiles were placed on the plate surfaces and a test conducted with semi-rigid specimens. Based on the thermopile measurements, Rennex [4] ascribed an estimate for the sampling uncertainty to be 0.015 K.

Thank You for previewing this eBook

You can read the full version of this eBook in different formats:

- HTML (Free /Available to everyone)
- PDF / TXT (Available to V.I.P. members. Free Standard members can access up to 5 PDF/TXT eBooks per month each month)
- Epub & Mobipocket (Exclusive to V.I.P. members)

To download this full book, simply select the format you desire below

